Desalination and Water Treatment
www.deswater.com

doi: 10.5004/dwt.2018.22896

129 (2018) 69–83
October

Pervaporation performance of silico-manganese nanohybrid/PU mixed matrix membranes for separation of phenol from water

Hong Ye[a,b,*], Chunxuan Dong[a], Qiufeng Zhu[a], Xiang Yan[a], Shengpeng Shi[c]

[a]*Key Laboratory of Cleaner Production and Integrated Resource Utilization of China National Light Industry, Beijing Technology and Business University (BTBU), Beijing 100048, China, Tel. +86 68984307; Fax: +86 10 68984307; emails: yehcn@163.com (H. Ye), dcx951211@163.com (C. Dong), zhuqiufeng@th.btbu.edu.cn (Q. Zhu), 1073481046@qq.com (X. Yan)*
[b]*Beijing Engineering and Technology Research Center of Food Additives, Beijing Technology and Business University (BTBU), Beijing 100048, China*
[c]*Beijing Research Institute of Chemical Industry, Beijing 100013, China, Tel. +86 59202781; email: sspcn@163.com*

Received 19 January 2018; Accepted 29 July 2018

ABSTRACT

Preparing a mixed matrix membrane (MMM) is an effective method for modifying pervaporation membranes. In our study, a variety of silico-manganese nanohybrids (SMNH) were prepared and applied for the first time in the modification of a polyurethane (PU) pervaporation membrane. The structure and morphology of SMNH and its MMMs were characterized using Fourier-transform infrared spectroscopy, X-ray diffraction, scanning electron microscope, transmission electron microscopy, contact angles, and Brunauer–Emmett–Teller. Moreover, the separation performances of MMMs were tested for separating phenol from water. Also, the effects of silica content, particle loading, feed temperature, and concentration were investigated. It was found that the mesoporous structures of SMNH particles have good affinity for phenol. SMNH with 30 wt% silica that is prepared via a two-step method (T-Mn-Si(30)) can simultaneously increase permeability and selectivity. In detail, a PU membrane with thickness of 110 μm containing 1 wt% T-Mn-Si(30) and with size of 200 nm can increase flux from 18.6 to 24.7 kg·μm·m^{-2}·h^{-1} with an increase in the separation factor from 9.3 to 15.5 for 0.3 wt% phenol solution at 80°C. Loading more than 1 wt% reduces flux and the separation factor for the special structure of T-Mn-Si(30) that has a tiny fringe. Increasing feed temperature and concentration increases both flux and the separation factor. Therefore, SMNH is an effective modifier for the PU membrane used to separate phenol from water.

Keywords: Pervaporation; Silico-manganese nanohybrid; Polyurethane; Mixed matrix membrane

1. Introduction

Phenol is a common organic chemical used in many fields, such as pharmaceutical, plastic, and petrochemical industries [1], but phenol is also a potential threat to water resources and public health. Thus, the recovery or separation of phenol from water is a challenging topic in terms of both the economy and the environment. Traditional technologies that have been used to deal with phenolic wastewater include distillation [2], extraction [3], and adsorption [4]. Their applications are effective, but they are limited by the restricted feed concentration and additional posttreatment [5]. Pervaporation is a promising process for recovering phenol from water because it is clean and simple. In particular, pervaporation has higher separation efficiency and lower energy consumption [6], making it very attractive compared with traditional technologies. The key factor of pervaporation is the membrane materials.

* Corresponding author.

The available research has focused on pervaporation separation of phenol from water far less than that of ethanol from water. The three main kinds of membrane materials used to separate phenol/water mixtures are polydimethylsiloxane (PDMS) [7–10], polyether block amide (PEBA) [11–13], and polyurethane (PU) [14–17]. Among these, PDMS is a traditional hydrophobic membrane material, and its selectivity for phenol is not satisfactory. PEBA has obtained excellent permeability and selectivity in previous research, although it is not actually available on a commercial scale [18]. PU has a particularly high separation factor (over 1,000) for separating phenol from water, but it has a low flux (less than 10 $g \cdot m^{-2} \cdot h^{-1}$) [15,19]. The comprehensive separation performances of PU are between those of PDMS and PEBA. However, because PU has a good film-forming property, thermal stability, and versatile structure, it is a very promising material for phenol separation from water. Modification is necessary to enhance synthetic separation performances of the PU membrane. Incorporating some inorganic fillers into polymer to fabricate mixed matrix membranes (MMMs) is one of the most facile and efficient modification methods, and choosing a good filler for the polymer matrix is very important.

Manganese oxide (MnO_2) is a transition metal oxide and is considered to be the most attractive oxide material because of its environmental friendliness and the high abundance of Mn [20]. MnO_2 has been used in adsorption [21–23], catalytic oxidation [24], and capacitor electrodes [25]. The adsorption properties of MnO_2-based hybrid particles for separating heavy metal ions and phenol from water have been researched. In our previous work [26], a silico-manganese nanohybrid (SMNH) was used for Cu(II) adsorption from aqueous solution, and we found that nanohybrid particles have good adsorption capacity and lower pH dependency than pure MnO_2. In addition, Liu et al. [21] discovered that manganese/silicon tailing can remove phenol and phenylamine from coking wastewater. These studies showed that the silico-manganese hybrid material has porous structure and an affinity for aromatic compounds. Moreover, Peng et al. [24] used MnO_2 for catalytic phenolic compound degradation and observed preferential adsorption of phenolic compounds on MnO_2. In general, MnO_2 and its hybrid particles have the potential to be a modifier for pervaporation membranes used to separate phenol from water. To the best of our knowledge, MnO_2 and its hybrid particles have not yet been used in pervaporation.

In this study, we prepared mesoporous SMNH particles as modifiers to PU matrix membranes for use in phenol recovery from water. Silica doping was performed via hydrothermal coprecipitation and in a two-step method. The addition of silicon dioxide (SiO_2) is for two purposes: (1) SiO_2 doping enhances acid stability of hybrid particles [26], which should be considered because phenol/water mixtures are weakly acidic; and (2) SiO_2 is reported to be a good modifier to pervaporation membranes and shows affinity for phenol [17,27]. Thus, SMNH particles were obtained and added to PU to prepare MMMs. The particles and MMMs were characterized using scanning electron microscope (SEM), transmission electron microscopy (TEM), contact angles (CAs), and Brunauer–Emmett–Teller (BET). Separation performances of MMMs for pervaporation separation of phenol from water were tested under different feed temperatures and concentrations, and effects of modifiers on separation performances were studied systematically.

2. Experiment

2.1. Materials

Potassium permanganate ($KMnO_4$), manganese sulfate monohydrate ($MnSO_4 \cdot H_2O$), and hexadecyl trimethyl ammonium bromide (CTAB) were obtained from Sinopharm Chemical Reagent Co., Ltd., China. Sodium silicate nonahydrate ($Na_2SiO_3 \cdot 9H_2O$) and phenol were provided by Tianjin Guangfu Fine Chemical Research Institute, China. Polyether (polytetrahydrofuran)-based PU (TX180) was purchased from Bayer Corporation, Germany. All the above reagents were of analytical grade and used without further purification. N,N′-dimethyl acetylamide (DMAc, analytical grade) was purchased from Beijing Huihaikeyi Co., Ltd., China. In addition, DMAc was purified by distillation under a reduced pressure over calcium hydride and stored over molecular sieves (4Å) before using.

2.2. Preparation of SMNH particles

2.2.1. Preparation of δ-MnO_2 (MnO_2)

The synthesis of δ-MnO_2 was carried out according to our previous work [28]. 2.0000 g of $KMnO_4$ was dissolved in 80 mL of deionized water, then 40 mL of $MnSO_4$ solution containing 0.3565 g of $MnSO_4 \cdot H_2O$ was pipetted dropwise into the solution of $KMnO_4$ under fast stirring. Then the as-obtained homogeneous solution was transferred into a 150 mL Teflon-lined stainless steel autoclave that was sealed and maintained at 160°C for 24 h. After the reaction was completed, the resulting solid product was filtered, washed with deionized water to remove ions and other possible remnant in the final products, and finally dried at 110°C overnight. The as-synthesized black fine powder was the mesoporous δ-MnO_2.

2.2.2. Preparation of SMNH particles via a hydrothermal coprecipitation method (Co-Mn-Si)

The synthesis of Co-Mn-Si was performed according to our previous work [28]. 0.0100 g of CTAB was dissolved in 80 mL of homogeneous solution with 2,000 g of $KMnO_4$ and 0.3565 g of $MnSO_4 \cdot H_2O$. A certain amount of $Na_2SiO_3 \cdot 9H_2O$ was put into 40 mL of deionized water, and then was added dropwise to the above purple suspension. The subsequent procedures were same as those in δ-MnO_2 preparation. The final product was assigned as Co-Mn-Si(*n*) with "*n*" representing the weight fraction that SiO_2 accounted for in the composite (SiO_2 + MnO_2), for example, Co-Mn-Si(30) refers to an SMNH containing 30 wt% of silica prepared via coprecipitation.

2.2.3. Preparation of SMNH particles via a two-step method (T-Si-Mn)

The synthesis of SMNH via two-step method was conducted as follows:

The as-obtained δ-MnO_2 (1.5 g) was dispersed into 80 mL of deionized water containing 0.5 wt% CTAB under an ultrasound treatment for 20 min. Then, $NaSiO_3 \cdot 9H_2O$ solution (14.4600 g $NaSiO_3 \cdot 9H_2O$ in 80 mL deionized water) was added

dropwise to the above δ-MnO_2 suspension in 80°C water bath with agitation. After the addition of the $NaSiO_3 \cdot 9H_2O$ solution, the subsequent procedures were same as those in δ-MnO_2 preparation. The final product was assigned as T-Mn-Si(*n*) with "*n*" representing the weight ratio of silica within the composite, for example, T-Mn-Si(30) referred to an SMNH containing 30 wt% of silica prepared via two-step method.

2.3. Preparation of MMMs

The membranes were all prepared by casting solution. PU (3.0000 g) was dissolved in DMAc (28 mL) to obtain a homogeneous solution. Then the required amount of the as-prepared SMNH particle was added in the above PU membrane solution under a magnetic stirring and a sonication. Finally, the membrane solution thus obtained was cast on a Teflon® plate and left under 80°C for 2 h, then thermally cured under vacuum at 120°C for 5 h to remove the residual solvent. The screw micrometer (Mitutoyo, 293–230 series, ±1 μm, Japan) was used to measure the thickness of membranes, and the average thickness obtained from five points was about 100 μm. Blank PU membrane was prepared by casting the pristine PU solution, and the rest of process was the same as MMMs. MMMs was assigned as PU/*X* (m wt%) with "*X*" and "m wt%" representing the added particle type and the particle loading, for example, PU/T-Mn-Si(30) (1 wt%) refers to PU membranes modified with 1 wt% T-Mn-Si(30).

2.4. Characterization of the nanohybrid and the modified PU membranes

2.4.1. Fourier-transform infrared spectroscopy

Fourier-transform infrared spectroscopy (FTIR) was used to determine the chemical composition of samples. The powder samples were tested by Nicolet IS10 (Thermo Scientific, USA) with the KBr pellet technique. The scanning was done in the range of 400–4,000 cm^{-1}.

2.4.2. TEM, SEM, and element analysis

TEM and mapping was conducted with a JEOL JEM-2010F operated at 200 kV equipped with energy dispersive X-ray spectroscopy (EDX) mapping. Elemental distribution maps were investigated using SEM (FEI Tecnai G2 F20) equipped with an energy dispersive spectrometer (EDS). The particles were ultrasonically dispersed in high-purity ethanol and then deposited onto the ultra-thin carbon-coated nickel grids.

The surface at airside and cross-section morphologies of the MMMs were observed by a high-resolution SEM of an FEI-XL30 field-emission SEM. The samples of cross section of membranes were obtained by breaking the specimens after freezing in the liquid nitrogen.

2.4.3. X-ray diffraction

The crystallinity of particles was analyzed by an X-ray diffraction (XRD) (Bruker D8 ADVANCE, Cu Kα radiation, λ = 1.5406 nm, Germany). The scanning was in the range of 10°–90° at a speed of 4°/min.

2.4.4. Surface and pore properties characterization

Nitrogen adsorption–desorption measurements conducted with an ASAP 2010 surface are an analyzer (Micrometrics Instrument Corporation, USA). All samples were pretreated in vacuum at 100°C for 2 h prior to analysis.

2.5. Adsorption experiment of particles

50 mg of certain kind of the particles was mixed with the phenol solution (200 g, 5 wt%) into flasks. Then, the flasks were shaken at a speed of 200 rpm at 20°C. When the adsorption equilibrium was reached, the suspension was filtered with a 0.45 μm membrane filter. The as-obtained liquid samples were determined for concentration using gas chromatography (GC9790II, Fuli Instruments, China).

The equilibrium uptake was determined using the mass balance equation:

$$Q = \frac{M\left(C_i - C_e\right)}{m} \tag{1}$$

where Q is the phenol amount adsorbed by kinds of particles at equilibrium state (mg g^{-1}), M is the mass of solution used in the adsorption experiment, C_i and C_e are the initial and equilibrium mass concentrations of phenol, and m is the mass of nanohybrid particle.

After the adsorption experiment, the particles were separated by the centrifugation. The slurry was dried in oven under atmosphere at 25°C for 48 h, and then put under vacuum at 25°C for 24 h to remove residual water and phenol. The dried particles were collected for XRD characterization.

2.6. CA measurement of membranes

The surface properties of membranes were characterized by CA using a CA instrument (JY-PHb, Jinhe Instrument Manufacturing Co., Ltd, Chengde, China). The test liquids of deionized water and 1 wt% phenol solution were applied. The average CA was obtained from four points on a sample with the sessile drop technology. The time of wetting was 20 s, because longer time would induce the local deformation of samples.

2.7. Pervaporation experiments

The pervaporation performances of the membranes were tested by using an apparatus from Tiandabeiyang Co., Ltd. (Tianjin, China) as shown in Fig. 1. The feed was heated and circulated from the feed tank (volume of 1.5×10^{-3} m^3) through the upstream side of the membrane cell by a pump with adjustable function of flow rate. A membrane supported by a porous sintered stainless steel in the permeate side was mounted in the pervaporation cell. The measurements were carried out for phenol/water mixtures in which the content of phenol was from 0.3–1.3 wt%. The feed mixture was maintained at temperature between 40°C and 80°C using a thermostat. The effective area of the membrane was 2.2×10^{-3} m^2. Vacuum on the permeate side was maintained below 200 Pa. Two cold traps were set in sequence:

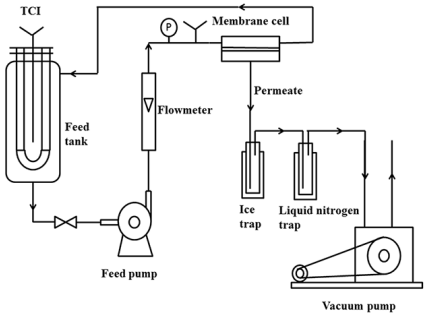

Fig. 1. Pervaporation test apparatus.

the first trap was the ice bath where most phenol was frozen to solid; the second one is the liquid nitrogen bath where the residual solvents from the last trap were totally captured. The concentrations of permeate and feed mixture were analyzed by the GC. The permeability was evaluated by the normalized flux (J, kg·μm·m^{-2}·h^{-1}) as defined in Eq. (2) to compare pervaporation performances of membranes with different thickness. Where Q (kg) is the total mass of permeate collected through the effective area of membrane (A, m^2) during the time t (h), and l is the membrane thickness (μm). The selectivity of membrane was demonstrated by separation factor (α) and defined as Eq. (3). Where Y_A and Y_B represent the weight fractions of phenol and water in the downstream permeate, and X_A and X_B represent those in the feed mixture, respectively. In order to evaluate the comprehensive separation performances of membranes considering the permeation and selectivity together, pervaporation separation index (PSI) was introduced and defined as Eq. (4). The average value was obtained from at least three repeated experiments for analysis.

$$J = \frac{Q}{A \times t} \times l \tag{2}$$

$$\alpha = \frac{Y_A \times X_B}{X_A \times Y_B} \tag{3}$$

$$\mathrm{PSI} = J \times (\alpha - 1) \tag{4}$$

In order to decouple the effect of driving force and compare the intrinsic properties of different membranes, the permeability was defined as Eq. (5).

$$P_i = \frac{J_i l}{x_{n,i}\gamma_i p_i^{\mathrm{sat}} - y_{n,i} p^p} \tag{5}$$

where P_i is the permeability of the component i, l is membrane thickness, $x_{n,i}$ and $y_{n,i}$ are the mole fractions of the component i in the feed and permeate, γ_i is the activity coefficient, p_i^{sat} is saturated vapor pressure, and p^p is permeate pressure. p_i^{sat} and γ_i are calculated from ASPEN ONE 7.2, respectively.

The partial vapor pressure of each component at the feed side can be expressed in terms of fugacity (f_i) as shown in Eq. (6). The driving force for the component i to transport through the membrane is the difference of its partial vapor pressures at the feed side and permeate side as shown in Eq. (7). If the pressure at the permeate side is very low and negligible considering the application of the vacuum pump, f_i can represent the driving force of component i.

$$f_i = x_{n,i}\gamma_i p_i^{\mathrm{sat}} \tag{6}$$

$$\text{Driving force} = x_{n,i}\gamma_i p_i^{\mathrm{sat}} - y_{n,i} p^p \tag{7}$$

Based on the above definition, the intrinsic selectivity can be defined as Eq. (8).

$$\beta = \frac{Pi}{Pj} \tag{8}$$

3. Results and discussion

3.1. Characterization of SMNH particles and SMNH-modified PU membranes

3.1.1. TEM, SEM, and element analysis

FTIR results prove the presence of MnO_2 and SiO_2, and XRD results provide the corresponding crystalline properties. FTIR and XRD results are shown in the supporting file. However, these results cannot provide concrete evidence of the hybrid MnO_2/SiO_2 structure. Thus, TEM and SEM with element analysis were used for further characterization.

TEM and SEM images of particles are shown in Figs. 2 and 3. As seen in Fig. 2, the average sizes of particles range from 200 to 500 nm and have diverse shapes. MnO_2 has urchin-like nanoparticles with thin sheet edges. Co-Mn-Si(30) presents many needle-like structures, and T-Mn-Si(30) is a kind of quasi-spherical particle that has tiny and spiny fringe. A two-step method seems to maintain more of the original shape of MnO_2 because MnO_2 and SiO_2 are formed separately. With an increase in silica content, SMNH particles obtained using the two-step method tend to detach in piece structures, as seen in Figs. 2(c)–(e). As seen in Fig. 2(f), EDX mapping of T-Mn-Si(30) shows that Mn and Si elements are spreaded all over the material. Similar mapping can be found for Co-Mn-Si(30) in Fig. S3 in the supplementary file. This implies that there is a uniform distribution of elements and real incorporation of SiO_2 in MnO_2. In addition, SEM + EDX was used to investigate the content of Si and Mn, and the results are shown in Fig. S4 and Table S1 in the supplementary file. T-Mn-Si(30) shows that the Si/Mn ratio is higher than that in Co-Mn-Si(30), and this means that more silica is present inside Co-Mn-Si(30), whereas more silica spreads on the surface of T-Mn-Si(30) to some extent.

SEM images of the cross section and surface of MMMs are shown in Fig. 3. We find that cross section of PU has a smooth texture (Fig. 3(a)). As seen in the cross-sectional images (Figs. 3(b) and (c)), the morphology does not change for the MMMs with 0.6 and 1 wt% T-Mn-Si(30), and the images show small aggregations. When the content of T-Mn-Si(30) is increased to 1.5 wt%, extensive aggregation

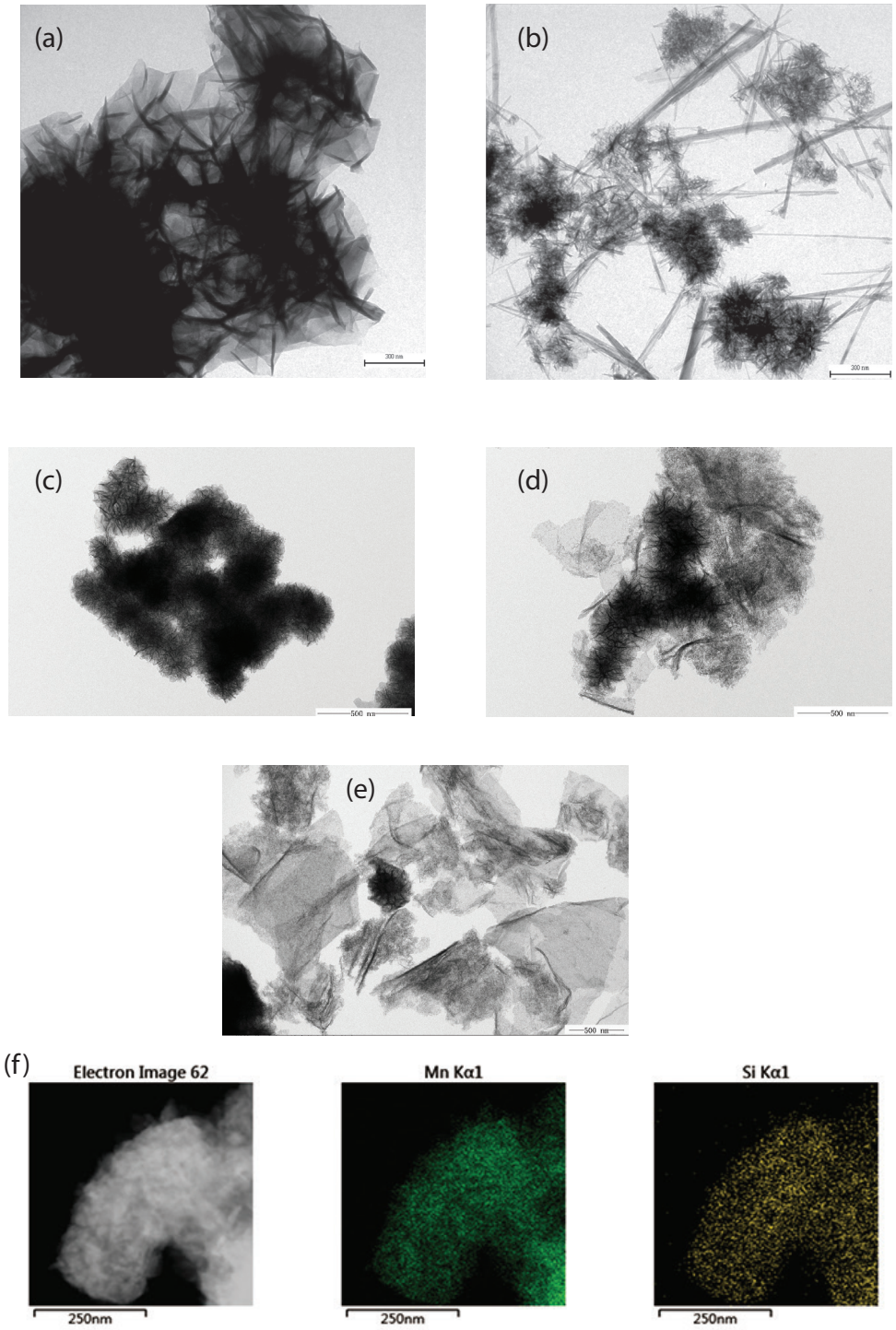

Fig. 2. TEM images of MnO_2 and SMNH particles: (a) MnO_2, (b) Co-Mn-Si(30), (c) T-Mn-Si(30), (d) T-Mn-Si(50), (e) T-Mn-Si(75), and (f) EDX mapping of T-Mn-Si(30).

appears. The appearance of aggregates could be due to the difference in polarity between SMNH and the soft segment of poly(tetrahydrofuran) because the former is an inorganic metal oxide with –OH, and the latter is more hydrophobic. It is known that aggregation of mixed fillers worsens the separation performance of a membrane [29–32], and thus, the content of SMNHs used in this study is less than 1.5 wt%.

3.1.2. Nitrogen adsorption and desorption isotherm

Nitrogen adsorption–desorption experimental results are shown in Table 1 and Fig. 4. As shown in Table 1, Co-Mn-Si(30) has higher surface area than MnO_2, which means that both MnO_2 and SiO_2 formed independently and resulted in separate particles. However, for T-Mn-Si(30), lower surface area

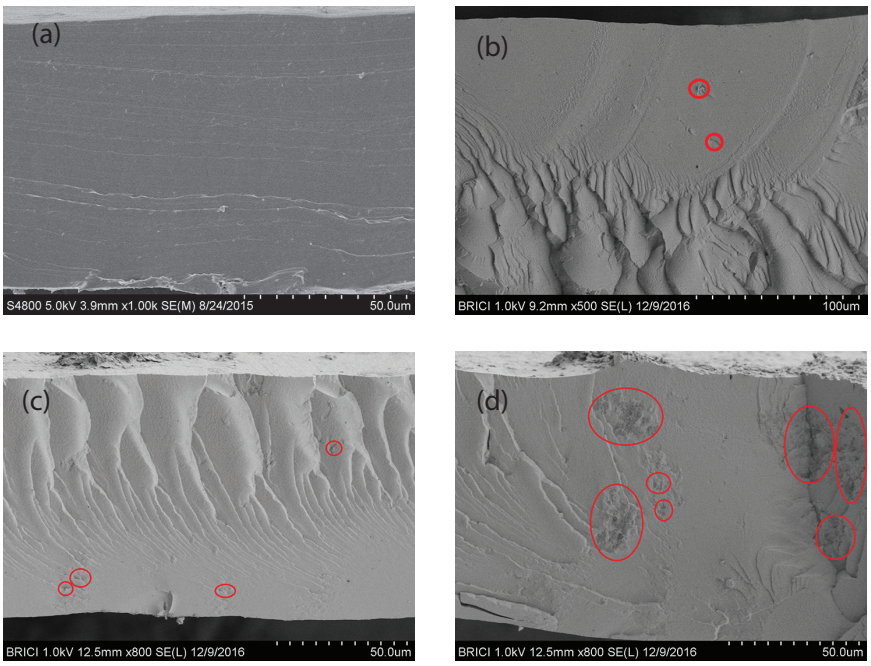

Fig. 3. SEM images of T-Mn-Si(30)-modified PU membranes: (a) PU, (b) PU/T-Mn-Si(30)(0.6 wt%), (c) PU/T-Mn-Si(30)(1.0 wt%), and (d) PU/T-Mn-Si(30)(1.5 wt%).

Table 1
Specific areas and pore characteristics of particles

	MnO_2	Co-Mn-Si(30)	T-Mn-Si(10)	T-Mn-Si(30)	T-Mn-Si(50)	T-Mn-Si(75)
Surface area, S_{BET} ($m^2 \cdot g^{-1}$)	38.02	258.40	39.06	45.09	87.50	121.30
Pore diameter, D_{BJH} (nm)	3.45	3.82	3.52	3.72	13.91	18.61
Pore volume, V_p ($cm^3 \cdot g^{-1}$)	0.088	0.668	0.086	0.103	0.277	0.357

BJH, Barrett–Joyner–Halenda method.

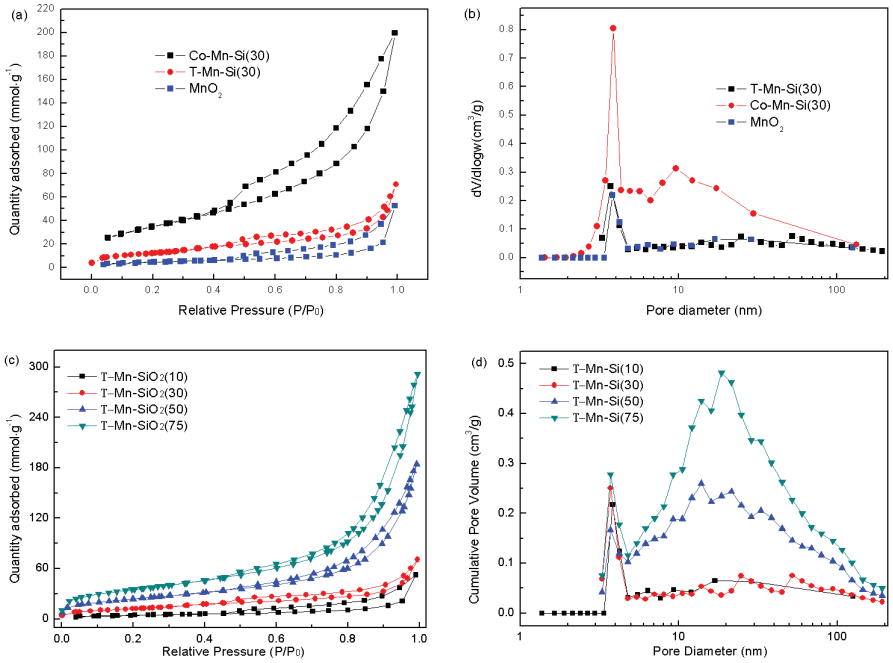

Fig. 4. (a) and (c), Nitrogen adsorption and desorption isotherms; and (b) and (d), pore size distributions.

and pore volume were obtained than Co-Mn-Si(30), and this implies that SiO_2 was deposited on the MnO_2 particles. Thus, the separation between MnO_2 and SiO_2 in T-Mn-Si becomes obvious because the surface area and pore volume increase with an increase in SiO_2 content. This implies that SiO_2 contributes mostly to the mesostructure of the hybrid particles of T-Mn-Si. Pores with sizes greater than 10 nm (in Figs. 4(b) and (d)) may result from interparticle pores.

As seen in Fig. 4(a), a type IV (Brunauer-Deming-Deming-Teller classification) isotherm with a hysteresis loop (especially for Co-Mn-Si(30)) can be assigned to the H_3 type. The more obvious trend in the H_3 loop is demonstrated in Fig. 4(c) for the compound with higher silica content. An H_3 loop means that there are narrow slit-shaped mesopores in the particles, and this is consistent with TEM results. In contrast, MnO_2 and T-Mn-Si(30) tend to have an H_4 type of loop [33], and this implies that conical pores are present. These pores may be generated from the intrinsic structure induced by the crystal structure of MnO_2 and micelles of CTAB. Such pores have relatively small sizes, as shown in Table 1. The different surface areas and pore distributions have great effects on the separation performances of modified membranes.

3.1.3. Adsorption characteristics of SMNH particles and CAs of membranes

The wettability of membranes was investigated using CA, which reflects the selectivity of membranes for solvent. The overall selectivity of a pervaporation membrane is considered to be mainly attributed to solution selectivity, and diffusion selectivity is generally lower than solution selectivity [34]. As seen in Fig. 5, all of the membranes have higher CAs with water and relatively lower CAs with 1 wt% phenol solution, and this means that the membranes have higher affinity for phenol. The differences between the CAs for water and phenol solution are about 3°–10°, except for PU/T-Mn-Si(30) (1 wt%), which has a difference of 27.6°, and this implies that PU/T-Mn-Si(30) (1 wt%) has the highest affinity for the feed solution.

Fig. 6 compares the equilibrium uptake of different SMNH particles. Three kinds of particles show preferential uptake for phenol. Relatively, T-Mn-Si(30) has the highest uptake of phenol followed by Co-Mn-Si(30), and MnO_2 has the lowest uptake. The electronegativity value of Si is 1.90 (Pauling unit), and the electronegativity value of Mn is 1.55 (Pauling unit) [35]. Higher electronegativity means stronger interaction with the electron cloud of phenol, and thus, SMNH particles perform better than MnO_2 in the phenol adsorption experiment. Under the same silica content, T-Mn-Si(30) shows higher equilibrium uptake than Co-Mn-Si(30). On one side, T-Mn-Si(30) probably has higher affinity for phenol, as reflected by Fig. 5; on the other side, higher pore volume of Co-Mn-Si(30) may be false because of interparticle pores, which can partly vanish if particles merged in solution.

3.2. PV performances of membranes

3.2.1. Effects of types of particles and silica content in particles

Separation performances of modified PU membranes were tested, and the results are shown in Fig. 7. For comparison, the flux was normalized for the membrane thickness. The types of particles and silica content in particles have great effects on separation efficiency.

As shown in Fig. 7(a), SMNHs/PU MMMs have higher flux and a higher separation factor than pristine PU and MnO_2-modified PU. In particular, PU/T-Mn-Si(30) has a total flux of 24.7 $kg{\cdot}\mu m{\cdot}m^{-2}{\cdot}h^{-1}$ and a separation factor of 15.5, where those of pure PU are 18.6 $kg{\cdot}\mu m{\cdot}m^{-2}{\cdot}h^{-1}$ and 9.3. As seen in Fig. 7(b), the addition of particles induces a greater increment of phenol flux than water. The good modification effect of SMNHs can be attributed to two factors: (1) SMNHs have good affinity for phenol, and (2) higher surface area of SMNHs helps increase the phenol flux. The separation factor and flux of MMM containing Co-Mn-Si(30) are lower than those of T-Mn-Si(30), and this is because of the lower affinity of the former than the latter. For all of this, both SMNHs improve the synthetic separation properties of PU.

Figs. 7(c) and (d) show the effects of silica content on separation characteristics. In general, total/partial fluxes and separation factors increase and then decrease with an increase in silica content from 0% to 75%. T-Mn-Si-modified membranes have a higher separation factor than Co-Mn-Si, and this is because of a more rapid increase in phenol flux of T-Mn-Si-modified membranes (Fig. 7(d)). T-Mn-Si(30) has the best modification effect and is used as the modifier for further study.

3.2.2. Effects of particle loading on separation performances

Fig. 8 shows the effects of T-Mn-Si(30) loading on the pervaporation performance. The total flux and separation

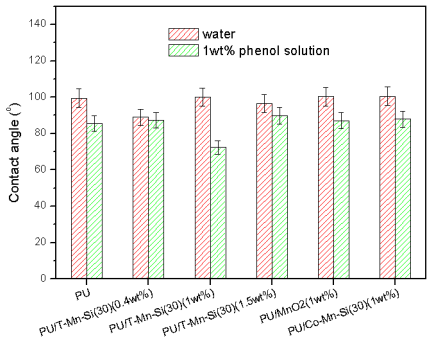

Fig. 5. Contact angles of PU and modified PU membranes.

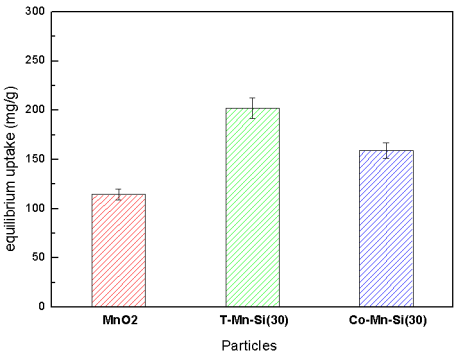

Fig. 6. Phenol uptake of particles.

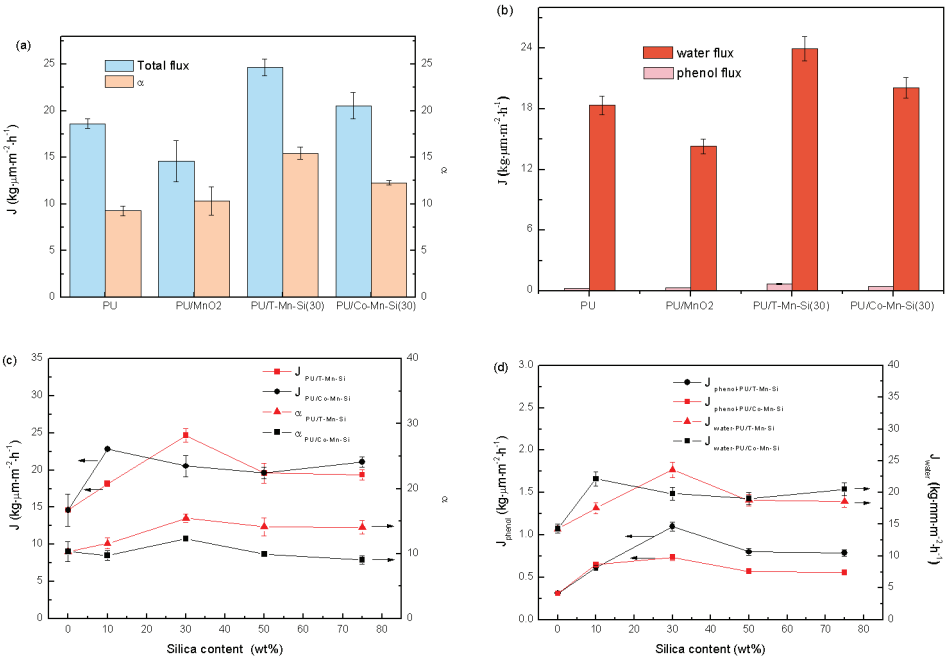

Fig. 7. Separation performances of PU and modified PU membranes (feed: 0.3 wt% phenol solution at 80°C, particle loading: 1 wt%). (a)and (b), Effects of types of particles; and (c) and(d) effects of silica content in particles.

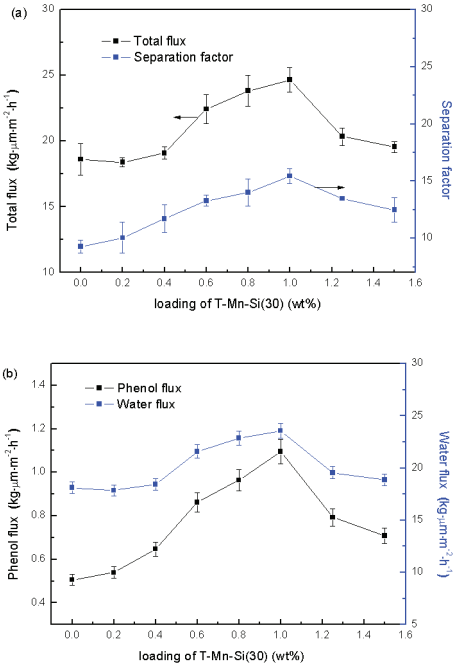

Fig. 8. Effects of T-Mn-Si(30) loading on separation performance of PU/T-Mn-Si(30): (a) separation factor and total flux and (b) partial flux (feed: 0.3 wt% phenol solution at 80°C).

factor for the pristine PU membrane are 18.6 kg·μm·m^{-2}·h^{-1} and 6.3, respectively. After incorporating T-Mn-Si(30), both the flux and separation factor increase synchronously and reach maximum values (24.7 kg·μm·m^{-2}·h^{-1} and 15.5, respectively) at 1.0 wt% loading and, decrease under higher loadings. From Fig. 8(b), we find a similar variation trend as seen in Fig. 8(a). Phenol flux increases from 0.5 to a maximum of 1.1 kg·μm·m^{-2}·h^{-1}, and water flux increases from 18.1 to a maximum of 23.6 kg·μm·m^{-2}·h^{-1} at 1 wt% loading. The increase in the inflection point at 1 wt% can be explained using the CA results and SEM images. On one hand, MMM with 1 wt% T-Mn-Si(30) has higher affinity for phenol than MMM with 0.4 and 1.5 wt% T-Mn-Si(30); on the other hand, a SEM image of the cross section of the membrane shows that higher loading (more than 1 wt%) of T-Mn-Si(30) results in aggregation (Fig. 3(d)). It is known that nonselective inner voids in aggregates worsen selectivity [36–38], and thus, the separation factor decreases with loading greater than 1 wt%. In many reports [13,36,38–42], flux continued to increase when particle aggregation occurred because more voids in aggregates were introduced. Here, total flux of T-Mn-Si(30)-modified PU also decreases with higher loading (more than 1 wt%), and this is probably because of the special morphology of T-Mn-Si(30). T-Mn-Si(30) has a quasi-spherical structure with tiny and spiny fringe, and it is quite different from sphere modifiers that have a smooth surface. The rough and spiny edge of T-Mn-Si(30) could be an obstacle for solvent diffusion. The possible mechanism of solvents permeating through aggregates is illustrated in Fig. 9. The tiny bumps of T-Mn-Si(30) edges interweave with each other and shrink the voids in the aggregates. Thus, a tortuous diffusion path is constructed. In contrast, for common spherical particle aggregates, the inner holes of aggregates are larger than those in T-Mn-Si(30). For an interfacial channel between particles and polymer, the spiny edge plays a similar role as the narrow interfacial gap. Thus, aggregate formation of T-Mn-Si(30) decreases the flux of the PU membrane.

3.2.3. Effects of feed concentration and temperature

Investigations of the effects of modifiers on separation performances were carried out under the same feed temperature and concentration. When the temperature

and concentration change, permeability and selectivity (as defined in Eqs. (5) and (8)) should be used to characterize separation performances to decouple the driving force.

Fig. 10 shows that with an increase in phenol content from 0.3 to 1.3 wt%, both the total and partial fluxes of PU/T-Mn-Si(30) (1.0 wt%) increase. Phenol flux increases from 1.1 to 2.1 kg·μm·m^{-2}·h^{-1}, and water flux increases from 23.6 to 34.4 kg·μm·m^{-2}·h^{-1}. Phenol flux increases more rapidly than water flux, and thus, the separation factor increases. The above variations in the apparent separation performances are usually ascribed to membrane swelling under higher feed concentration. If the driving force of solvents from flux were eliminated, the data would be quite different. As shown in Table 2, the activity coefficient (57.49) of phenol is more than 57 times that of water (1.00). However, the saturated vapor pressure (2.0 kPa) and molar fraction (5.76 × 10^{-4} mol%) for phenol are much less than those of water. In particular, the molar fraction of water is almost 1,736 times greater than that of water, and mathematically, this results in a driving force for phenol across the membrane that is much lower than water, which affects the permeability greatly. As shown in Fig. 10(c), phenol permeability decreases from 16.8 to 8.7 kg·μm·m^{-2}·h^{-1}·kPa^{-1}, whereas water permeability increases from 0.5 to 0.7 kg·μm·m^{-2}·h^{-1}·kPa^{-1}. This induces a decrease in intrinsic selectivity from 33.7 to 11.9 in Fig. 10(d) with an increase in concentration. In fact, PU/T-Mn-Si(30) shows much higher permselectivity to phenol than water. The low driving force of phenol can compensate for the high phenol permeability of the membrane when we evaluate membrane performances using only apparent phenol flux.

In addition, phenol permeability decreases with an increase in phenol concentration. This is mathematically understandable because the increasing degree of the driving force for phenol is higher than the increasing degree of phenol flux. There may be two explanations for this. On one hand, more phenol–phenol and phenol–water clusters might form in the mixture that contains more phenol, and these clusters have larger kinetic diameter than water clusters [43]. On the other hand, reduced phenol permeability may be due to a crowding (saturation) effect of phenol diffusion through T-Mn-Si(30) pores, as suggested by Baker et al. [44].

Fig. 11(a) shows that total flux, partial fluxes, and the separation factor increase simultaneously with an increase in temperature. Fig. 11(b) shows that the permeabilities of

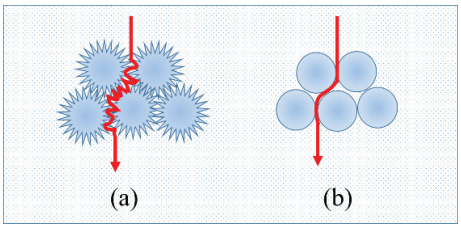

Fig. 9. Permeation path through different aggregates in a membrane: (a) quasi-spherical and (b) spherical.

Table 2
Water and phenol at 80°C in 0.3 wt% phenol aqueous solution

Component	Mol %	Molecular weight (g/mol)	Saturated vapor pressure (kPa)	Activity coefficient
Phenol	5.76 × 10^{-4}	94.11	2.0	57.49
Water	9.99 × 10^{-1}	18.02	47.4	1.00

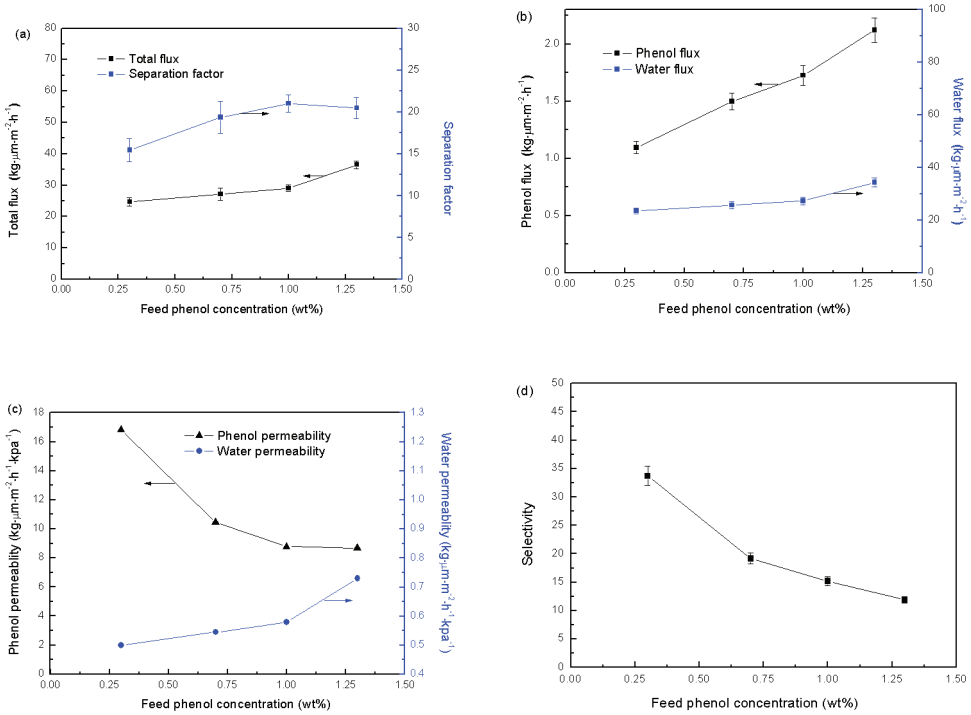

Fig. 10. Effects of feed concentration on separation performances of PU/T-Mn-Si(30): (a) total flux and separation factor, (b) phenol and water flux, (c) permeability, and (d) selectivity (loading: 1 wt%, feed temperature: 80°C).

phenol and water decrease with an increase in temperature. This is understandable according to Eq. (5), because the driving force for the solvents increases with an increase in temperature.

The above temperature dependence of partial flux and permeability can be plotted using the Arrhenius equation as follows:

$$J = J_0 \exp\left(\frac{-E_a}{RT}\right) \tag{9}$$

$$P = P_0 \exp\left(\frac{-E_P}{RT}\right) \tag{10}$$

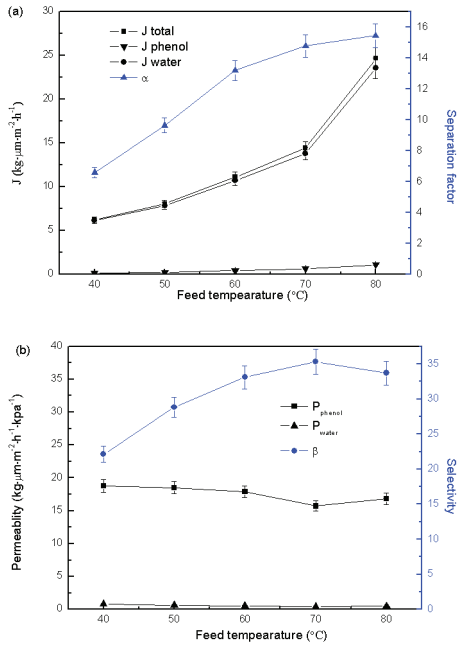

Fig. 11. Effects of feed temperature on separation performances of PU/T-Mn-Si(30): (a) flux and separation factor and (b) permeability and selectivity (loading: 1 wt%, feed content: 0.3 wt%).

where J_0 and P_0 are pre-exponential factors, R is the universal gas constant, T is the operating temperature, and E_a and E_p are the apparent activation energies of flux and permeability, respectively. E_a and E_p were calculated, and the results are shown in Table 3. E_a is positive, and E_p is negative, and these values indicate the degree and direction of temperature effects on flux and permeability. Feng and Huang [45] suggested that the difference between E_a and E_p is the molar enthalpy of vaporization (ΔH_v), which is expressed as follows:

$$\Delta H_v = E_a - E_p \tag{11}$$

Thus, ΔH_v values of phenol and water are calculated as 53.2 and 43.1 kJ/mol. The reference values for these are 55.1 kJ/mol for phenol and 45.1 kJ/mol for water, which are higher than the ΔH_v values calculated using Eq. (11). The prerequisite for Eq. (11) is that the permeate pressure ($y_{n,i}p^p$) is very low compared to $x_{n,i}\gamma_i p_i^{sat}$ in Eq. (7) and is neglected in the derivation. Omitting $y_{n,i}p^p$ induces some error between the values of ΔH_v calculated from Eq. (11) and the reference values.

3.2.4. Comparison of data reported in the literature

The pervaporation performances of MMMs obtained in our study are compared with those of other hybrid membranes discussed in the literature and listed in Table 4. The separation factor and flux are both important for membrane application. Thus, PSI was adopted here to combine these two factors for a comprehensive evaluation of membranes. PSI values obtained with the present MMMs are much higher than those

Table 3
Activity energy (kJ/mol) of solvents

Component	E_a	E_p	$\Delta H_v = E_a - E_p$	Reference value (ΔH_v)[a]
Phenol	49.7	–3.5	53.2	55.1
Water	29.8	–13.3	43.1	45.1

[a]Reference value is the mean value of ΔH_v at 40°C–80°C calculated using Aspen.

Table 4
Pervaporation performance of membranes for the separation of phenol aqueous solution

Membrane	Feed concentration (wt%)	Feed temperature (°C)	Thickness (μm)	Total flux (kg·m^{-2}·h^{-1})	Separation factor	PSI (kg·m^{-2}·h^{-1})	References
PDMS	2	70	50[a]	0.4	11.6	4.2	[46]
Polyimide	1	70	1	2	12.5	23	[47]
PIM-1	1	70	40	0.21	16	3.2	[48]
PU	5	60	150	0.007	75	0.5	[19]
PUU(1% LiCl)	3	75	–	0.028	119	3.3	[14]
PEBA	0.8	70	50	0.85	39	32.3	[13]
PEBA(10% ZIF-8)	0.8	70	50	1.31	53	67.6	[13]
PU/T-Mn-Si(30) (1%)	1.3	80	105	0.37	20.5	7.2	This work
PU/T-Mn-Si(30) (1%)	1.0	80	100	0.29	21.0	5.8	This work

[a]Effective thickness of selective layer. PIM, Polymers of intrinsic microporosity; PUU, polyurethaneurea; ZIF, zeolitic imidazolate framework.

of most other membranes. PEBA has excellent comprehensive separation performance for recovery of phenol from water. However, the casting process of the PEBA membrane solution has to be carried out on a heated plate to ensure a homogeneous solution, and PEBA is not available on a commercial scale [18]. Polyimide also shows good performance, although preparing polyimide membranes with a thickness of 1 μm is quite difficult. By comparison, the film-forming operation of the SMNH-modified PU in our work can be conveniently conducted at room temperature. Hence, the SMNH-modified PU membrane is promising for separating phenol from water, and SMNH is a new and effective material for modifying membranes. Moreover, SMNH is environmentally friendly and easier to prepare than popular modifiers such as metal-organic frameworks and graphene oxide.

4. Conclusions

SMNH particles and SMNH-modified MMMs were prepared in this work. Mesoporous structures of SMNH particles have good affinity for phenol in adsorption and CA experiments. T-Mn-Si(30) simultaneously increases permeability and selectivity. In detail, adding 1 wt% T-Mn-Si(30) to PU increases flux from 18.6 to 24.7 kg·μm·m^{-2}·h^{-1} and increases the separation factor from 9.3 to 15.5 for 0.3 wt% phenol solution at 80°C. Loading more than 1 wt% T-Mn-Si(30) reduces flux and the separation factor because of the special structure of T-Mn-Si(30) with tiny fringe. Increasing the feed temperature and concentration increases both flux and the separation factor. Therefore, SMNH is an effective modifier to PU membranes that are used in separating phenol from water.

Acknowledgment

The authors gratefully acknowledge The National Key R&D Program of China (2017YFC1600605), Beijing Natural Science Foundation (2172020), construction of technological innovation and service capability-basic scientific research service fee-innovation platform of grain and oil food supply chain hazard identification and early warning technology (PXM2018_014213_000033), and National Natural Science Foundation of China (No. 21503007).

Symbols

PU	—	Polyurethane
SMNH	—	Silico-manganese nanohybrid
MnO_2	—	Manganese oxide
SiO_2	—	Silicon dioxide
Co-Mn-Si(n)	—	Silico-manganese nanohybrid particles obtained via coprecipitation, n: weight fraction of SiO_2 in SMNH
T-Mn-Si(n)	—	Silico-manganese nanohybrid particles obtained via two-step method, n: weight fraction of SiO_2 in SMNH
J	—	Total flux (kg•μm•m^{-2}•h^{-1})
J_i	—	Partial flux of the component i (kg•μm•m^{-2}•h^{-1})
α	—	Separation factor
PSI	—	Pervaporation separation index
T	—	Feed temperature
P_i	—	Permeability of the component i (kg•μm•m^{-2}•h^{-1}•kPa^{-1})
$x_{n,i}$	—	Mole fraction of the component i in the feed
$y_{n,i}$	—	Mole fraction of the component i in the permeate
γ_i	—	Activity coefficient of i component
p_i^{sat}	—	Saturated vapor pressure (kPa)
p^p	—	Permeate pressure (kPa)
f_i	—	Fugacity of i component (kPa)
β	—	Selectivity
E_a	—	Apparent activation energy of flux (kJ•mol^{-1})
E_p	—	Permeability activation energies (kJ•mol^{-1})
ΔH_v	—	Molar enthalpy of vaporization (kJ•mol^{-1})

References

[1] A. Krastanov, Z. Alexieva, H. Yemendzhiev, Microbial degradation of phenol and phenolic derivatives, Eng. Life Sci., 13 (2013) 76–87.
[2] Y. Zhuo, Y. Zhong, Y. Xu, Y. Sha, Evaluation of transfer resistances in the reactive distillation process for phenol production, Ind. Eng. Chem. Res., 55 (2015) 257–266.
[3] A. Kargari, Phenol removal from aqueous solutions by a novel industrial solvent, Chem. Eng. Commun., 202 (2015) 408–413.
[4] S.H. Lin, R.S. Juang, Adsorption of phenol and its derivatives from water using synthetic resins and low-cost natural adsorbents: a review, J. Environ. Manage., 90 (2009) 1336.
[5] M.A. Hararah, K.A. Ibrahim, A.H. Al-Muhtaseb, R.I. Yousef, A. Abu-Surrah, A. Qatatsheh, Removal of phenol from aqueous solutions by adsorption onto polymeric adsorbents, J. Appl. Polym. Sci., 117 (2010) 1908–1913.
[6] Y.M. Xu, T. Chung, High-performance UiO-66/polyimide mixed matrix membranes for ethanol, isopropanol and n-butanol dehydration via pervaporation, J. Membr. Sci., 531 (2017) 16–26.
[7] S.J. Han, F.C. Ferreira, A. Livingston, Membrane aromatic recovery system (MARS) – a new membrane process for the recovery of phenols from wastewaters, J. Membr. Sci., 188 (2001) 219–233.
[8] P. Wu, R.W. Field, R. England, B.J. Brisdon, A fundamental study of organofunctionalised PDMS membranes for the pervaporative recovery of phenolic compounds from aqueous streams, J. Membr. Sci., 190 (2001) 147–157.
[9] P. Wu, R.W. Field, B.J. Brisdon, R. England, S.J. Barkley, Optimisation of organofunction PDMS membranes for the pervaporative recovery of phenolic compounds from aqueous streams, Sep. Purif. Technol., 22–23 (2001) 339–345.
[10] H. Ye, X. Yan, X. Zhang, W. Song, Pervaporation properties of oleyl alcohol-filled polydimethylsiloxane membranes for the recovery of phenol from wastewater, Iran. Polym. J., 26 (2017) 639–649.
[11] X. Hao, M. Pritzker, X. Feng, Use of pervaporation for the separation of phenol from dilute aqueous solutions, J. Membr. Sci., 335 (2009) 96–102.
[12] C. Li, X. Zhang, X. Hao, X. Feng, X. Pang, H. Zhang, Thermodynamic and mechanistic studies on recovering phenol crystals from dilute aqueous solutions using pervaporation–crystallization coupling (PVCC) system, Chem. Eng. Sci., 127 (2015) 106–114.
[13] C. Ding, X. Zhang, C. Li, X. Hao, Y. Wang, G. Guan, ZIF-8 incorporated polyether block amide membrane for phenol permselective pervaporation with high efficiency, Sep. Purif. Technol., 166 (2016) 252–261.
[14] B. Sinha, U.K. Ghosh, N.C. Pradhan, B. Adhikari, Separation of phenol from aqueous solution by membrane pervaporation using modified polyurethaneurea membranes, J. Appl. Polym. Sci., 101 (2006) 1857–1865.

[15] T. Gupta, N.C. Pradhan, B. Adhikari, Separation of phenol from aqueous solution by pervaporation using HTPB-based polyurethaneurea membrane, J. Membr. Sci., 217 (2003) 43–53.
[16] S. Das, A.K. Banthia, B. Adhikari, Porous polyurethane urea membranes for pervaporation separation of phenol and chlorophenols from water, Chem. Eng. J., 138 (2008) 215–223.
[17] H. Ye, J. Wang, Y. Wang, X. Chen, S. Shi, Effects of simultaneous chemical cross-linking and physical filling on separation performances of PU membranes, Iran. Polym. J., 22 (2013) 623–633.
[18] W. Kujawski, A. Warszawski, W.O. Ratajczak, T. Porbski, W.A. Capa, A.I. Ostrowska, Application of pervaporation and adsorption to the phenol removal from wastewater, Sep. Purif. Technol., 40 (2004) 123–132.
[19] T. Gupta, N.C. Pradhan, B. Adhikari, Synthesis and performance of a novel polyurethaneurea as pervaporation membrane for the selective removal of phenol from industrial waste water, Bull. Mater. Sci., 25 (2002) 533–536.
[20] N. Izyumskaya, Y. Alivov, S.J. Cho, H. Morkoc, H. Lee, Y.S. Kang, Processing, structure, properties, and applications of PZT thin films, Crit. Rev. Solid State Mater. Sci., 32 (2007) 111–202.
[21] H. Liu, S. Gao, M. Zhu, P. Chen, D. Pan, Use of manganese/silicon tailing waste for coking wastewater treatment: evaluation of phenol and phenylamine removal efficiencies, Water Air Soil Pollut., 226 (2015) 78.
[22] S.A. Younis, Y.M. Moustafa, Synthesis of urea-modified $MnFe_2O_4$ for aromatic micro-pollutants adsorption from wastewater: mechanism and modeling, Clean Technol. Environ. Policy, 19 (2017) 527–540.
[23] G.D.F. Lima, V.S. Ferreira, N.V. Godoy, R.F. Medeiros, F.M.D.S. Garrido, E.S. Ribeiro, S. Nakagaki, M.G. Segatelli, M.A. Bezerra, C.R.T. Tarley, Study of silica-manganese oxide hybrid material as a new solid phase for on-line continuous flow enrichment of Cd(II) ions coupled to flame atomic absorption spectrometry, Microchem. J., 109 (2013) 98–105.
[24] W. Peng, S. Wang, X. Li, Shape-controlled synthesis of one-dimensional α-MnO_2 nanocrystals for organic detection and pollutant degradation, Sep. Purif. Technol., 163 (2016) 15–22.
[25] T. Yeo, D. Shin, J. Shin, H. Hwang, B. Seo, J. Lee, W. Choi, DC-field-driven combustion waves for one-step fabrication of reduced manganese oxide/multi-walled carbon nanotube hybrid nanostructures as high-performance supercapacitor electrodes, J. Mater. Chem. A, 5 (2017) 24707–24719.
[26] Q. Zhu, L. Wang, Z. An, H. Ye, X. Feng, Hydrothermal synthesis of silico-manganese nanohybrid for Cu(II) adsorption from aqueous solution, Appl. Surf. Sci., 371 (2016) 102–111.
[27] M.L. Sforca, I. Yoshida, C.P. Borges, S.P. Nunes, Hybrid membranes based on SiO_2/polyether-b-polyamide: morphology and applications, J. Appl. Polym. Sci., 82 (2001) 178–185.
[28] Q. Zhu, L. Wang, Z. An, H. Ye, X. Feng, Hydrothermal synthesis of silico-manganese nanohybrid for Cu(II) adsorption from aqueous solution, Appl. Surf. Sci., 371 (2016) 102–111.
[29] X. Cheng, F. Pan, M. Wang, W. Li, Y. Song, G. Liu, H. Yang, B. Gao, H. Wu, Z. Jiang, Hybrid membranes for pervaporation separations, J. Membr. Sci., 541 (2017) 329–346.
[30] Y.M. Xu, T. Chung, High-performance UiO-66/polyimide mixed matrix membranes for ethanol, isopropanol and n-butanol dehydration via pervaporation, J. Membr. Sci., 531 (2017) 16–26.
[31] G. Wu, M. Jiang, T. Zhang, Z. Jia, Tunable pervaporation performance of modified MIL-53(Al)-NH_2/poly(vinyl alcohol) mixed matrix membranes, J. Membr. Sci., 507 (2016) 72–80.
[32] D. Hua, Y.K. Ong, Y. Wang, T. Yang, T. Chung, ZIF-90/P84 mixed matrix membranes for pervaporation dehydration of isopropanol, J. Membr. Sci., 453 (2014) 155–167.
[33] K.S.W. Sing, Reporting physisorption data for gas/solid systems, Pure Appl. Chem., 57 (1985) 603–619.
[34] H. Morinaga, Mechanism of metallic particle growth and metal-induced pitting on Si wafer surface in wet chemical processing, J. Electrochem. Soc., 141 (1994) 2834–2841.
[35] D. Sun, P. Yang, L. Li, H.H. Yang, B.B. Li, Poly(dimethylsiloxane)-poly (tetrafluoroethylene)/poly (vinylidenefluoride) (PDMS-PTFE/PVDF) hollow fiber composite membrane for pervaporation of chloroform from aqueous solution, Korean J. Chem. Eng., 31 (2014) 1877–1884.
[36] G. Zhang, J. Li, N. Wang, H. Fan, R. Zhang, G. Zhang, S. Ji, Enhanced flux of polydimethylsiloxane membrane for ethanol permselective pervaporation via incorporation of MIL-53 particles, J. Membr. Sci., 492 (2015) 322–330.
[37] G. Liu, Z. Jiang, K. Cao, S. Nair, X. Cheng, J. Zhao, H. Gomaa, H. Wu, F. Pan, Pervaporation performance comparison of hybrid membranes filled with two-dimensional ZIF-L nanosheets and zero-dimensional ZIF-8 nanoparticles, J. Membr. Sci., 523 (2017) 185–196.
[38] G. Wu, M. Jiang, T. Zhang, Z. Jia, Tunable pervaporation performance of modified MIL-53(Al)-NH 2/poly(vinyl alcohol) mixed matrix membranes, J. Membr. Sci., 507 (2016) 72–80.
[39] Y. Zhang, N. Wang, C. Zhao, L. Wang, S. Ji, J. Li, $Co(HCOO)_2$-based hybrid membranes for the pervaporation separation of aromatic/aliphatic hydrocarbon mixtures, J. Membr. Sci., 520 (2016) 646–656.
[40] J.G. Varghese, R.S. Karuppannan, M.Y. Kariduraganavar, Development of hybrid membranes using chitosan and silica precursors for pervaporation separation of water + isopropanol mixtures, J. Chem. Eng. Data, 55 (2010) 2084–2092.
[41] W. Zhang, Y. Ying, J. Ma, X. Guo, H. Huang, D. Liu, C. Zhong, Mixed matrix membranes incorporated with polydopamine-coated metal-organic framework for dehydration of ethylene glycol by pervaporation, J. Membr. Sci., 527 (2017) 8–17.
[42] D. Hua, Y.K. Ong, Y. Wang, T. Yang, T. Chung, ZIF-90/P84 mixed matrix membranes for pervaporation dehydration of isopropanol, J. Membr. Sci., 453 (2014) 155–167.
[43] L.L. Ngoc, Y. Wang, T. Chung, Pebax/POSS mixed matrix membranes for ethanol recovery from aqueous solutions via pervaporation, J. Membr. Sci., 379 (2011) 174–183.
[44] R.W. Baker, J.G. Wijmans, Y. Huang, Permeability, permeance and selectivity: a preferred way of reporting pervaporation performance data, J. Membr. Sci., 348 (2010) 346–352.
[45] X. Feng, R.Y.M. Huang, Estimation of activation energy for permeation in pervaporation processes, J. Membr. Sci., 118 (1996) 127–131.
[46] P. Wu, R.W. Field, R. England, B.J. Brisdon, A fundamental study of organofunctionalised PDMS membranes for the pervaporative recovery of phenolic compounds from aqueous streams, J. Membr. Sci., 190 (2001) 147–157.
[47] F. Pithan, C. Staudt-Bickel, Crosslinked copolyimide membranes for phenol recovery from process water by pervaporation, Chemphyschem, 4 (2003) 967–973.
[48] P.M. Budd, E.S. Elabas, B.S. Ghanem, S. Makhseed, N.B. McKeown, K.J. Msayib, C.E. Tattershall, D. Wang, Solution-processed, organophilic membrane derived from a polymer of intrinsic microporosity, Adv. Mater., 16 (2004) 456–459.

Supplementary material

Fourier-transform infrared spectroscopy

As shown in Fig. S1, the broad and strong peak of 3,430 cm^{-1} is attributed to the stretching vibration of –OH, which implies abundant –OH on surface of these particles. Another peak at 1,627 cm^{-1} is normally owed to the O–H bending mode. Besides, the typical MnO_2 peak at 530 cm^{-1} can be observed for SMNH particles and pure MnO_2. As for the characteristic peak of SiO_2, T-Mn-Si(30) shows much more obvious band at 1,106 cm^{-1} than others and the shoulder peak at 1,200 cm^{-1} due to asymmetric Si–O–Si stretching vibration.

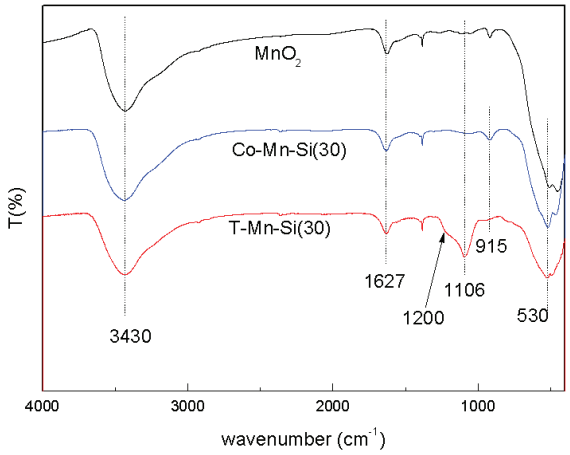

Fig. S1. Spectra of FTIR of SMNHs.

X-ray diffraction

X-ray diffraction (XRD) was used for characterizing the crystallinity of as-obtained particles. As shown in Fig. S2, δ-MnO_2 shows four sharp peaks at 12.4° (001), 28.8° (002), 36.7°(111), and 65.8° (311) ascribed to layered birnessite-type MnO_2 (JCPDS no. 80-1098) in good agreement with reported work. Comparing with δ-MnO_2, the positions of MnO_2 characteristic peaks in SMNHs are not changed, which means the crystal type of MnO_2 is not transformed. However, these peaks of SMNHs are weakened and broadened after SiO_2 doping, which implies the pristine MnO_2 crystal is destroyed, albeit to a small degree. Observing from the peaks of (001) and (002), the degree that the two peaks broaden for Co-Mn-Si(30) is greater than T-Mn-Si(30). That is because the precursors of MnO_2 and SiO_2 are mixed together during coprecipitation, while in two-step method the precursor of SiO_2 is added after MnO_2 solid has been obtained. Theoretically, the peaks owed to SiO_2 should be observed in XRD pattern, while they are hardly found with a little bolder line around 22.8° (amorphous silica) than MnO_2. That is because the SiO_2 peaks cannot be demonstrated under 30 wt% silica. When silica content is increased to 50%, the peak ascribed to SiO_2 becomes obvious as shown by Fig. S2(c). XRD result of particles which experienced adsorption experiments is also shown. Because the amount of samples after adsorption experiment is little and the color of particles is black and brown, the fluorescent signal will be comparable to X-ray diffraction one. That induces an obvious noise baseline in XRD curves. Even so, we can

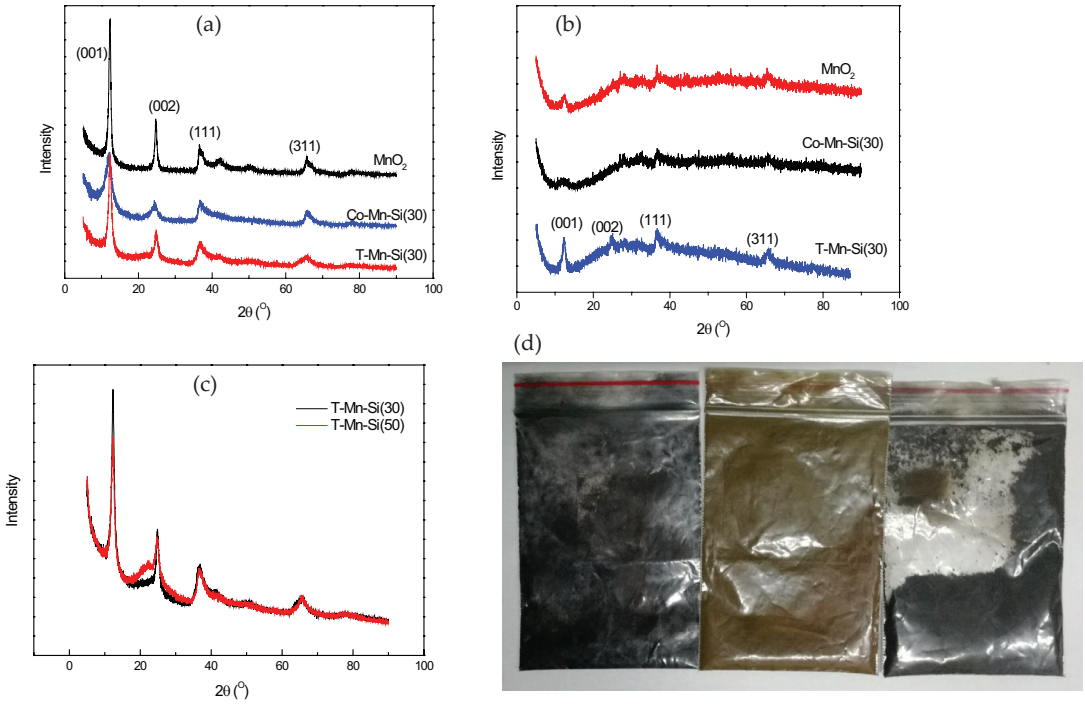

Fig. S2. XRD and digital photo of particles: (a) XRD pattern of pristine particles, (b) XRD pattern of particles after adsorption experiment, (c) XRD comparison of T-Mn-Si(30) and T-Mn-Si(50), and (d) digital photo of MnO_2, Co-Mn-Si(30), and T-Mn-Si(30).

observe that T-Mn-Si(30) keeps the characteristic peaks as the pristine one. While the corresponding peaks of MnO_2 and Co-Mn-Si(30) become weaker or even disappear, which proves good stability of T-Mn-Si(30) in phenol solution.

Morphologies of particles and membranes from TEM and SEM are shown in Fig. S3, Fig. S4 and Fig. S7.

The stability of membrane

From the point of industrial application of hybrid membrane, long-time stability of separation performance is expected. To investigate the stability of membrane performance, pervaporation test of PU/T-Mn-Si(30) (1 wt%) (129.6 μm) was carried out using 0.3 wt% phenol aqueous solution at 50°C during 3 d. In each day, pervaporation test lasts for 12 h, and the total experiment time is 72 h. In addition, in order to make the feed concentration constant, phenol concentration in feed mixture was monitored at intervals. Phenol will be added to feed tank if phenol concentration lowers. As shown in Fig. S6, the total flux and separation factor are relatively constant during operation time, which means SMNH modified membrane has good operation stability.

Table S1
Element contents of different particles in EDS

Samples	Si/Mn (atom ratio%)	Si/Mn (wt%)	Theoretical Si/Mn (wt%)	Theoretical Si/Mn+Si (wt%)
MnO_2	0	0	0	0
Co-Mn-Si(30)	5.19	2.62	23.12	30
T-Mn-Si(30)	28.3	14.48	23.12	30

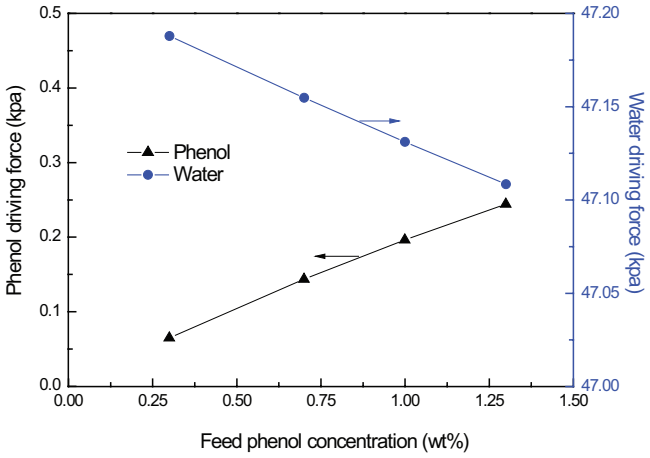

Fig. S5. Driving force with phenol concentration.

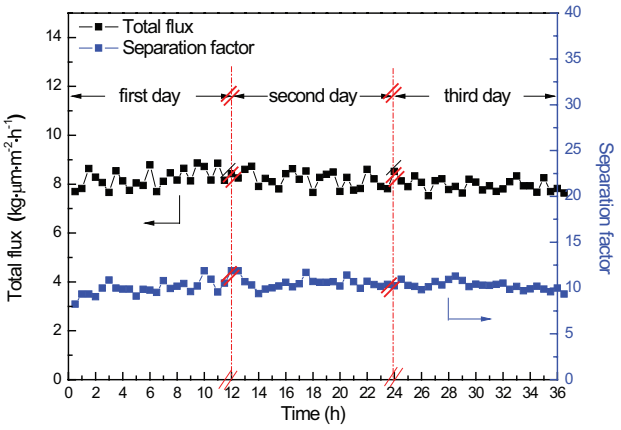

Fig. S6. Effects of operation time on pervaporation performances.

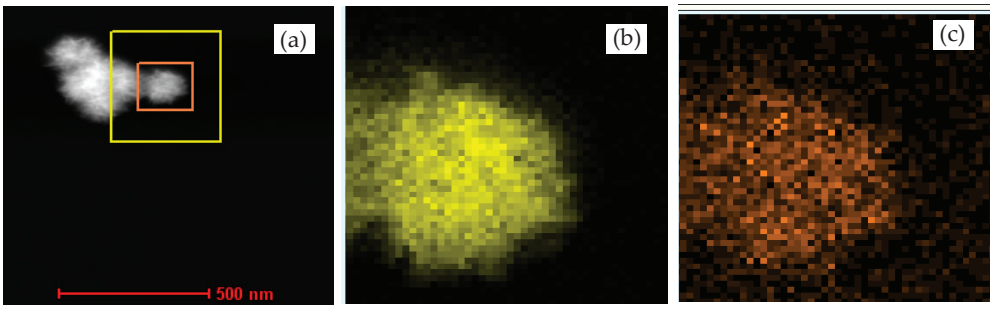

Fig. S3. EDX mapping of Co-Mn-Si(30): (a) scale and (b) Mn (c) Si.

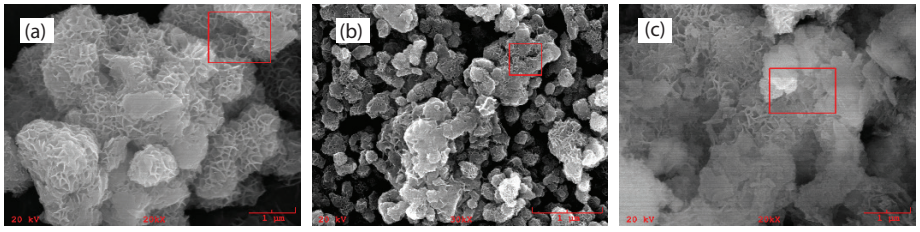

Fig. S4. SEM of different particles (the red rectangle is EDS scanning position): (a) MnO_2, (b) Co-Mn-Si(30), and (c) T-Mn-Si(30).

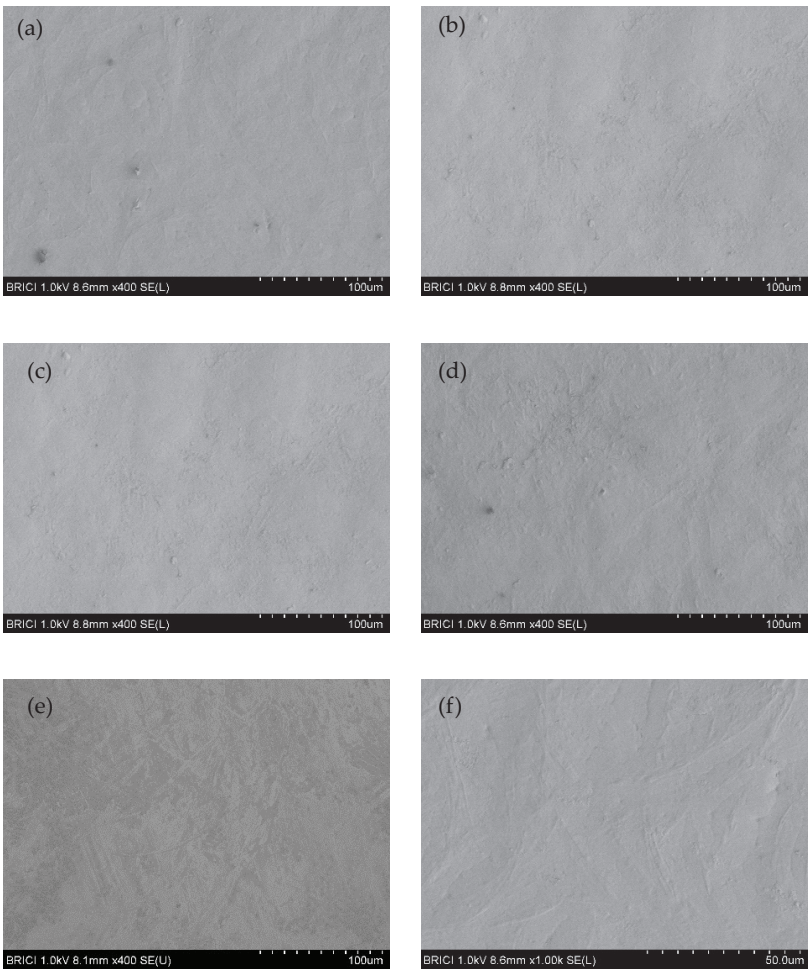

Fig. S7. SEM of surfaces of different membranes: (a) PU, (b) PU/T-Mn-Si(30) (0.6 wt%), (c) PU/T-Mn-Si(30) (1.0 wt%), (d) PU/T-Mn-Si(30) (1.5 wt%), (e) PU/MnO_2 (1.0 wt%), and (f) PU/Co-Mn-Si(30) (1.0 wt%).